Journal of Applied Polymer Science

A Method for Scale-Up of Co-Electrospun Nanofibers via Flat Core-Shell Structure Spinneret

Huihui Wu,[1] Yuansheng Zheng,[1] Yongchun Zeng[1,2]

[1]College of Textiles, Donghua University, Songjiang, Shanghai 201620, People's Republic of China

[2]Key Laboratory of Textile Science and Technology, Donghua University, Ministry of Education, Shanghai 201620, People's Republic of China

Correspondence to: Y. Zeng (E-mail: yongchun@dhu.edu.cn)

ABSTRACT: An approach to the scale-up of co-electrospinning via a flat core-shell structure spinneret has been developed in this study. The spinneret with a flat surface involves shell-holes and core-needles. Electric field simulation reveals that the flat core-shell spinneret configuration creates a more uniform electric field gradient. Experimental study shows that in comparison with the conventional needle co-electrospinning, core-shell nanofibers produced by this new designed setup are finer and of better morphology. Composite nanofibers with special morphologies can be fabricated by modifying the structure of this spinneret. The production rate of the core-shell nanofibers can be enhanced by increasing the hole and needle number of the spinneret. This novel design is expected to provide a promising method towards the massive production of core-shell nanofibers. © 2014 Wiley Periodicals, Inc. J. Appl. Polym. Sci. **2014**, *131*, 41027.

KEYWORDS: composites; electrospinning; fibers; nanostructured polymers

Received 9 February 2014; accepted 15 May 2014

DOI: 10.1002/app.41027

INTRODUCTION

Co-electrospinning is a new branch of nanotechnology bifurcated from the previously known electrospinning.[1,2] To broaden the nanofiber properties, researchers have introduced co-electrospinning (or coaxial elelctrospinning) for producing core-shell composite nanofibers with desired multi-functions.[3–6] Polymer solutions (in immiscible or miscible solvents) are supplied from a spinneret consisting of two coaxial capillaries. At the spinneret exit a core-shell droplet emerges and when the electricfield is sufficiently strong, jetting sets in at its tip. The core-shell structure is preserved in the out-flowing jet and co-electrospinning proceeds properly. The jet exhibits the electrically induced whipping initially discovered in electrospinning of single-fluid jets, which results in strong stretching of the bending sections of the jet.[7–10] The solvent eventually evaporates, the jet dries and solidifies, and as-spun fibers (with the core-shell structure and diameters typically in the submicron range) are deposited on acounter electrode.

In recent years, many researchers have attempted to enhance the production rate of electrospinning process in more sophisticated ways, such as increasing the number of spinning sites. The previously reported approaches can be generally classified based on the feed method at the spinning site: either a confined or unconfined fluid-volume feed.[11] In confined feed systems, the polymer solution is injected into enclosed capillaries such as needles,[12] holes,[13] and microfluidic channels.[14] Conversely, in unconfined feed systems, a polymer solution flows unconstrained over a free liquid surface.[15] The confined feeding systems have the advantage of maintaining a continuous stable electrospinning process, controlling the collection of the fiber mats, and controlling the fiber diameters due to the constrained injected rate of the solution. Moreover, the confined feeding method can produce fibers of special structures, such as core-shell fibers. Our previous work[16] developed a multihole system with a flat spinneret to scale up the productivity of electrospun nanofibers. We found that this multihole system created a more uniform electric field than the conventional multineedle system. On the basis of these findings, we consider scale-up co-electrospinning via modifying this multihole spinneret into a flat core-shell structure spinneret.

In the last several years, lots of papers on co-electrospinning and their applications have been published.[17] However, literatures referring to scale-up approaches for co-electrospinning have not been found. In a conventional co-electrospinning system, the spinneret involves core and shell metal needles with two compartments attached to corresponding syringes containing different polymer solutions.[18] Scaling up the productivity with this system by increasing the number of core and shell

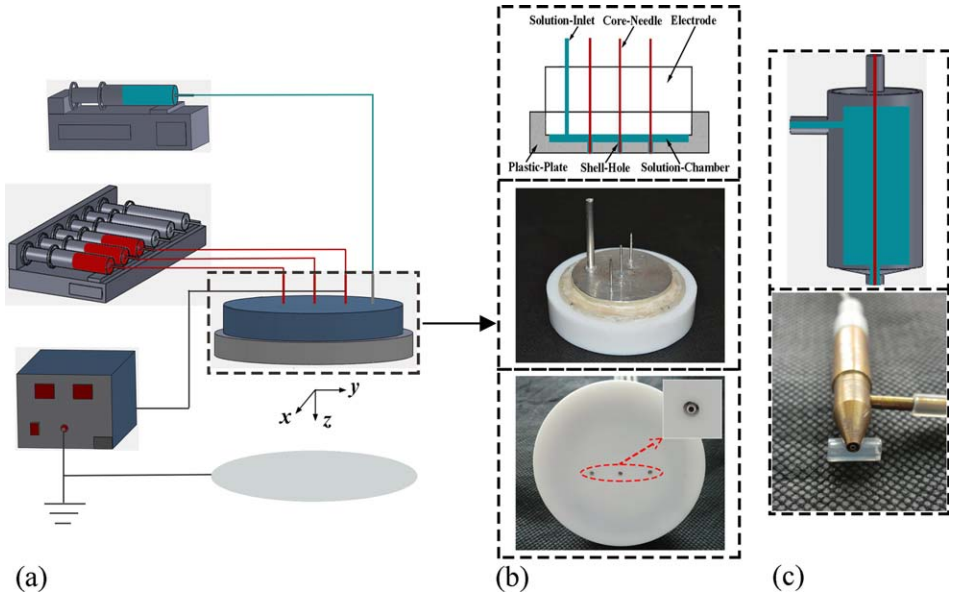

Figure 1. Schematic of the multiholeco-electrospinning system: (a) experimental setup (b) flat core-shell structure spinneret, and (c) conventional needle co-electrospinning spinneret. [Color figure can be viewed in the online issue, which is available at wileyonlinelibrary.com.]

needles may lead to complicated devices. In this study, a flat core-shell structure spinneret is developed to enhance the productivity and to improve fiber morphology of the electrospun core-shell nanofibers. Three-dimensional (3D) electric fields are simulated to understand the effects of electric field distribution on co-electrospinning. Meanwhile, experimental work is carried out to compare the spinning process and fiber morphology of this new design and the conventional needle co-elelctrospinning system.

EXPERIMENTAL

Material Preparation

Polystyrene (PS) ($M_w = 350{,}000$ g mol^{-1}, Aldrich); Elastane PU2180A10 ($M_w = 70{,}000$–$150{,}000$ g mol^{-1}, BASF); *N*,*N*-dimethylformamide (DMF) (0.945–0.950 g mL^{-1} at 20°C, Shanghai Chemical Reagents, China); All of these materials were used without further purification. Homogeneous PS solution and PU solution with the concentrations of 20 and 7 wt %, respectively were prepared by dissolving the corresponding pellets in DMF. The solution was prepared by gently stirring for 5 h with an electric mixer (AM200, Shanghai Only, China) and all experiments were performed at about 25°C in air at 40–60% RH.

Experimental Setup

The scheme of the designed multihole co-electrospinning system is shown in Figure 1. The novel spinneret (called flat core-shell structure spinneret) consists of an aluminum electrode and a plastic plate made of polytetrafluoroethylene (PTFE). The electrode is a cylinder with 50-mm diameter and 20-mm height. A 2-mm-outer-diameter tube was inserted into the electrode to provide shell solution feeding. The plastic plate with 2-mm thickness was used for creating the electrospinning jet. A solution chamber was formed between the electrode and the plastic plate. Holes (in this study, three holes were used) with 1.5-mm diameter were drilled in the plastic plate to eject shell solution. Blunt-type needles with 0.8-mm outer-diameter and 0.5-mm inner-diameter were inserted through the electrode and into the holes to eject core solution. The polymer solutions were forced from syringes via syringe pumps (KDS 220, KD Scientific, USA) to the spinneret. A voltage power supply (ES-60P 10W/DDPM, Gamma High Voltage Research, USA) was applied to the spinneret and the aluminum foil-grounded collector. For comparison, a conventional needle co-electrospinning spinneret is also shown [Figure 1(c)]. The core-needle is the same as the needle used in the flat spinneret, while the shell-needle is with the same inner-diameter of the hole in the flat spinneret.

Characterization

The morphology of the resultant core-shell fibers were observed under a Scanning Electron Microscope (SEM) (JS M- 560 0LV, Japan) after gold coating (coating time is 60 s). A Transmission Electron Microscope (TEM) (JEM-2100, JEOL, Japan) was used to study the internal morphology of the core-shell fibers. The average fiber diameter was calculated from the SEM images using Photoshop Cs 6 (Adobe System, San Jose, CA) software from a collection of 500 fibers.

Jet Path Record

A Redlake HG-100K high-speed camera (Redlake, San Diego, CA) equipped with a Nikon 24–85 mm, *f* 2.8 zoom lens was employed to record the jet motion during the co-electrospinning process. This camera has the capability of recording images at a frame rate up to 100,000 frames per second (f/s). The light source was two 2500 W lamps.

Electric Field Simulation

The 3D electric fields were analyzed by Ansoft Maxwell (ANSYS, USA) software using the finite element method (FEM). The electric field intensities were calculated by Ansoft Maxwell software. Before the calculation, the physical geometries of the co-electrospinning setups (e.g., electrode, PTFE spinneret, and

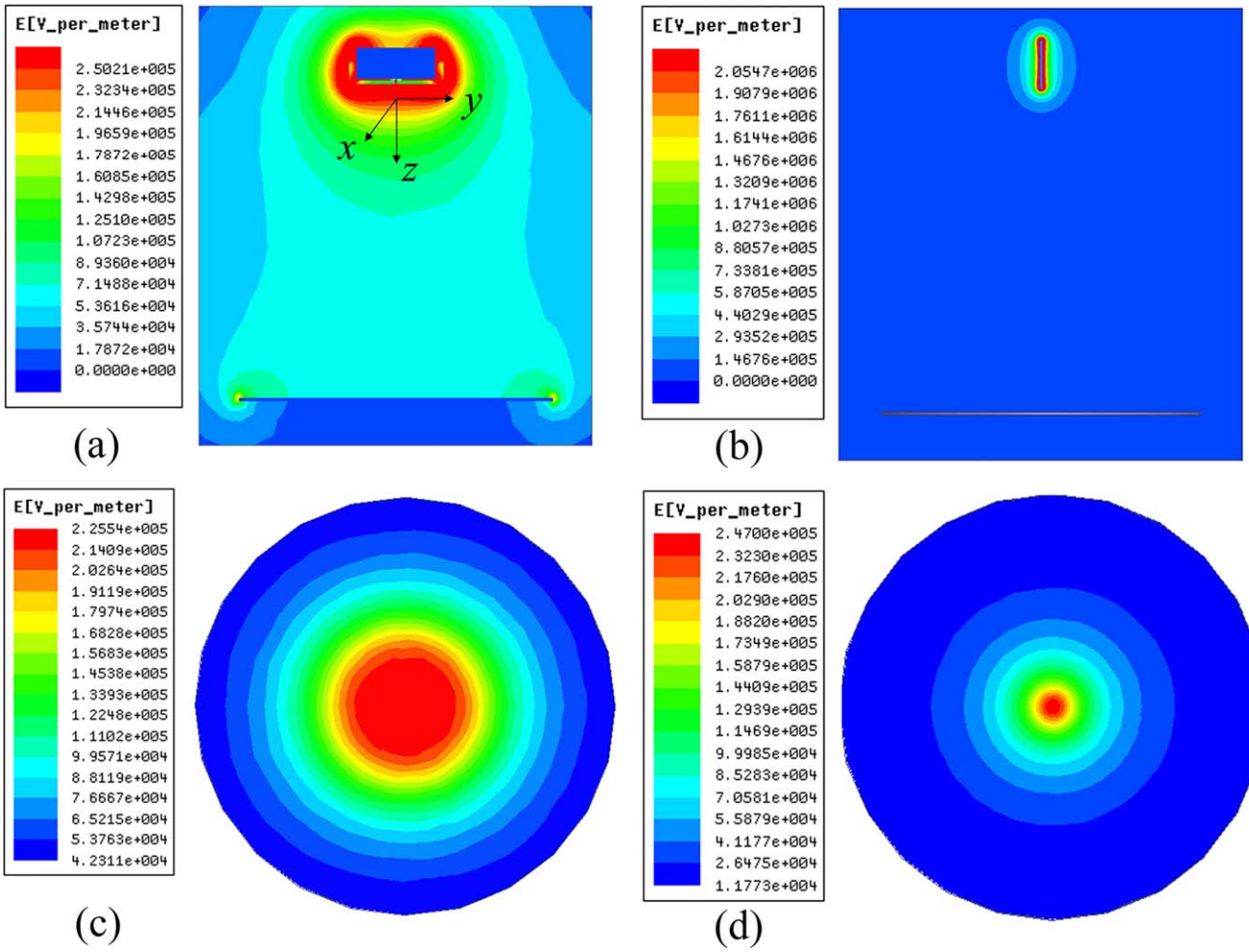

Figure 2. Comparison of the electric field distributions for the two systems under a working distance of 20 cm and an applied voltage of 20 kV: center plane along *z*-axis of (a) flat spinneret, (b) needle spinneret; *xy*-plane at $z = 10$ mm of (c) flat spinneret, and (d) needle spinneret. [Color figure can be viewed in the online issue, which is available at wileyonlinelibrary.com.]

collector) and polymer solutions were established according to their practical dimensions, locations, and relative permittivities.

RESULTS AND DISCUSSION

Electric Field Distribution

The 3D electric fields for both the flat core-shell configuration and the conventional needle co-electrospinning system were simulated. For comparison, the flat spinneret with single hole was used in the simulation. The simulations were under the conditions of 20-cm working distance and 20-kV applied voltage, which was used in the experiments for a stable spinning process. Figure 2 shows the simulated electric field distributions for the two systems under the same processing conditions of 20-cm working distance and 20-kV applied voltage. It can be seen that compared to the needle geometry, the flat spinneret [Figure 2(a)] creates a much more uniform electric field which changes gradually with the distance from the spinneret. As shown in [Figure 2(b)], an inhomogeneous electric field with an extremely high electric field concentrated in the surrounding area of the needle is created by the needle system. Figures 2(c,d) illustrate that the flat spinneret creates a much larger area of uniform electric field in the *xy* plane (the horizontal plane) at the position of $z = 10$ mm. These analyses can be quantified by the calculated data, as shown in Figure 3. [Figure 3(a)] shows the electric field intensity *E* along the spinning direction at centerline for the two co-electrospinning systems. In the needle configuration, *E* declines from the apex rapidly in the area near the spinneret, while the flat configuration creates a quite uniform electric field with a gradual decrease of *E*. At the distance of about $z = 10$ mm, the electric field intensity created by the flat configuration starts to exceed the needle configuration. Figure 3(b) shows the electric field intensity along the *y*-axis in the distance close to the spinneret ($z = 1$ mm) for the two co-electrospinning systems. It is important to find that the flat configuration creates a higher electric field except the area very close to the spinneret.

Jet Path Observation

Figure 4(a) shows the composite jets formed from the three-hole flat core-shell spinneret under the conditions of 20-cm working distance and 20-kV applied voltage. The PU-core solution was tinted with a commercial dye (0.01 wt %) to improve the imaging contrast. The droplet at the plate is shown to be a

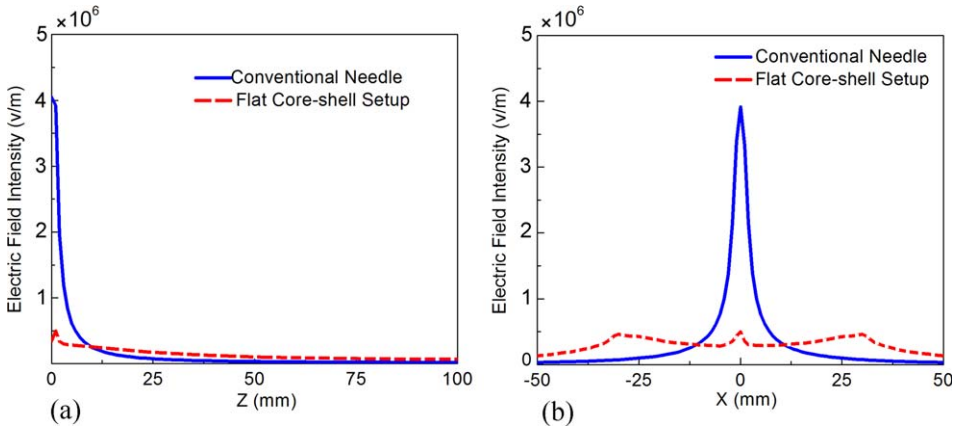

Figure 3. Electric field intensity for the two co-electrospinning systems with a working distance of 20 cm and an applied voltage of 20 kV: (a) *E* distribution along *z*-axis at central line and (b) *E* distribution along *y*-axis at $z = 1$ mm. [Color figure can be viewed in the online issue, which is available at wileyonlinelibrary.com.]

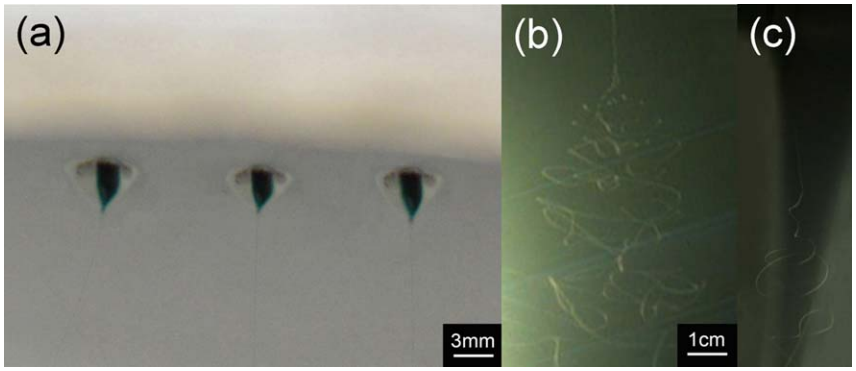

Figure 4. (a) Composite jets ejected from the three-hole flat core-shell spinneret, and jet path created by (b) flat core-shell spinneret co-electrospinning process, (c) single-fluid electrospinning process. [Color figure can be viewed in the online issue, which is available at wileyonlinelibrary.com.]

composite with core and shell solutions. The conical shape of the droplet becomes sharper and a composite jet emanates from the tip of the droplet, and the core-shell structure is preserved in the out-flowing jet.

Figure 4(b) shows the jet path created by the flat core-shell structure spinneret. As the case of the jet motion in a single-fluid electrospinning process, the composite jet goes through a straight section followed by a whipping instability. It is well known that the bending path in a single-fluid electrospinning process turns to be three-dimensional spiral loops, especially in the initial part of the whipping, as shown in Figure 4(c). We can see that compared to the single-fluid electrospinning, the bending path in the co-electrospinning process is more complex and less regular. This may result from the different conductivities, elastic modulus and viscosities of the two fluids.[19]

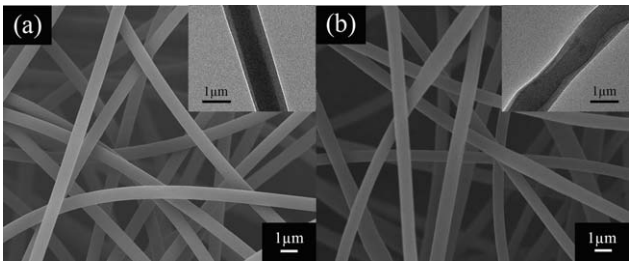

Figure 5. SEM and TEM images of the core-shell nanofibers obtained from (a) multihole flat core-shell and (b) needle co-electrospinning system. (The working distance is 20 cm and the applied voltage is 25 kV. The flow rate of the core-needle is 0.5 mL h^{-1} and the shell-needle/hole is 1.5 mL h^{-1}, respectively).

Fiber Diameter Distribution

Figure 5 shows the SEM images of the electrospun core-shell fibers obtained from the three-hole flat spinneret and conventional needle spinneret co-electrospinning systems with the 20-kV voltage and 20-cm working distance. The flow rate for the core-needle is 0.5 mL h^{-1}, and that for the shell-hole (or needle) is 1.5 mL h^{-1}. It is known that the uniform of the core-shell structures is one of the most important factors for the application of core-shell nanofibers. For example, the hollow fibers dissolved the core component and encapsulated with nano-particles could experience an efficient charge transportation, while the uniform of core component favors the accuracy of photocatalytic process.[20] The inserted TEM images in Figure 5 illustrate that the core fiber produced from the flat core-shell spinneret is more straight and uniform. From the SEM images, it is observed that the multihole flat spinneret produces a bit finer fibers. Fiber diameter distributions at various voltages are

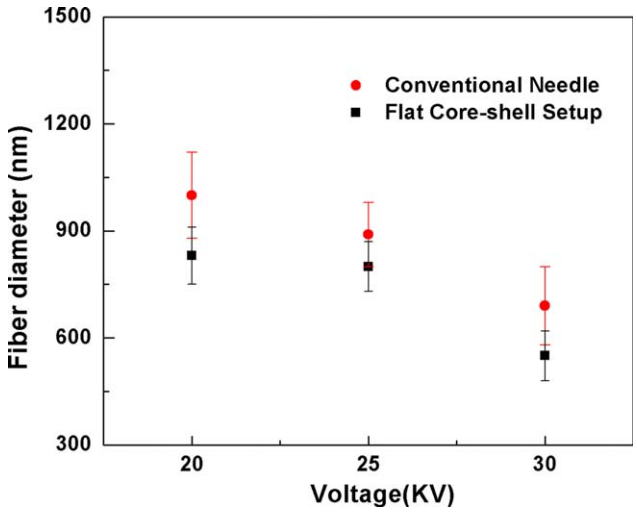

Figure 6. Fiber diameter distributions of the core-shell nanofibers obtained from the two co-electrospinning systems at various voltages. (The working distance is 20 cm and the flow rate of the core-needle is 0.5 mL h^{-1} and the shell-needle/hole is 1.5 mL h^{-1}, respectively). [Color figure can be viewed in the online issue, which is available at wileyonlinelibrary.com.]

shown in Figure 6. Under the same processing condition, the fibers obtained from the multihole flat core-shell setup are finer than those from the needle co-electrospinning setup. The fiber diameter decreases with increasing applied voltage for both the two systems. It has been shown in the simulation results that the flat configuration creates a higher electric field except the area very close to the spinneret. Therefore, the smaller fiber diameter produced by the flat spinneret may be resulted from the larger electric force due to the higher electric field intensity in the whipping region of the jet motion.

Special Morphology Fiber

Nanofibers with special structures, such as porous nanofibers, grooved nanofibers and nanosprings (or self-crimping nanofibers) have found various applications.[21,22] It was reported that grooved and micro-textured surfaces could provide directional cues for the morphogenesis of cells with a preferred direction.[23]

In this study, by adjusting the position of the core-needle in the shell-hole [Figure 7(a), in this case, the core-needles is off-centered], nanofibers with special structure can be obtained in a simple way. Figure 7(b) shows the SEM image of the grooved nanofibers in the fiber mat produced with the modified flat core-shell spinneret. The inserted SEM and TEM images show the detail structure of the grooved nanofibers. As can be noted, the fibers have remarkable grooves on their surfaces along the fiber axial both in width and depth. The typical fiber morphology of these fibers may be ascribed to the off-centered configuration and the shrinkage of core component. The same solvent for the core and shell component makes it easy to dissolve the thin side of the shell layer near the central needle.

Scale-Up Analysis

Under the same conditions, the productivity of the co-electrospinning setup is determined by the number of the jets. For the conventional needle co-electrospinning setup, the flow rates for the core-needle and the shell-needle are 0.5 and 1.5 mL h^{-1}, respectively. For the three-hole flat core-shell spinneret, the productivity is about three times of the needle setup, which is about 1.5 mL h^{-1} for the core-needles and 4.5 mL h^{-1} for the shell-holes. The production rate of core-shell fibers can be scaled up by increasing the hole and needle numbers.

CONCLUSIONS

A co-electrospinning setup for the scale-up of the core-shell nanofibers has been developed. We compared the electric field distribution and fiber morphology obtained from the conventional needle co-electrospinning system and the new designed flat core-shell structure spinneret configuration. The results indicate that the flat spinneret creates finer fibers with uniform core-shell structure due to more uniform electric field distribution. This method provides a promising method towards the massive production of core-shell nanofibers.

ACKNOWLEDGMENTS

This work was financially supported by the National Natural Science Foundation of China (11272088), the Keygrant Project of Chinese Ministry of Education (113027A), the Fundamental Research Funds for the Central Universities.

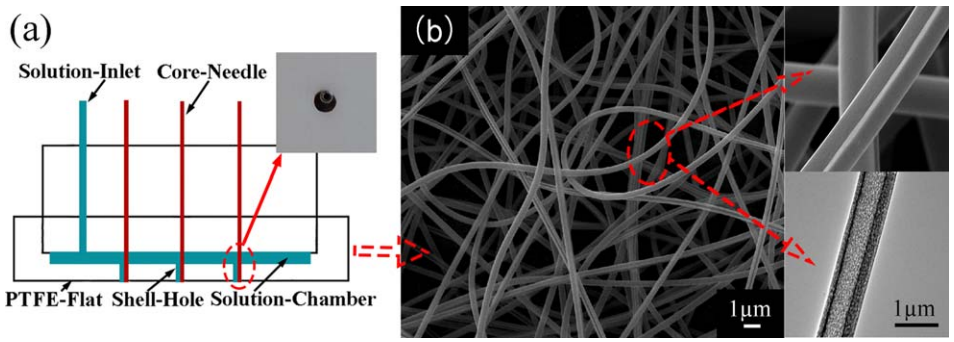

Figure 7. Special structure fibers: (a) schematic of the modified flat core-shell spinneret, (b) the SEM image of the produced grooved fibers (the inserted SEM and TEM images show the detail structure of the grooved nanofibers). (The working distance is 20 cm and the applied voltage is 20 kV. The flow rate of the core-needle is 0.5 mL h^{-1} and the shell hole is 1.5 mL h^{-1}, respectively). [Color figure can be viewed in the online issue, which is available at wileyonlinelibrary.com.]

REFERENCES

1. Loscertales, I. G.; Barrero, A.; Marquez, M.; Spretz, R.; Velarde-Ortiz, R.; Larsen, G. *J. Am. Chem. Soc.* **2004**, *126*, 5376.
2. Huang, Z. M.; Zhang, Y. Z.; Kotaki, M.; Ramakrishna, S. *Compos. Sci. Technol.* **2003**, *63*, 2223.
3. Agarwal, S.; Greiner, A.; Wendorff, J. H. *Prog. Polym. Sci.* **2013**, *38*, 963.
4. Qu, H. L.; Wei, S. Y.; Guo, Z. H. *J. Mater. Chem. A*, **2013**, *1*, 11513.
5. Sun, Z.; Zussman, E.; Yarin, A. L.; Wendorff, J. H.; Greiner, A. *Adv. Mater.* **2003**, *15*, 1929.
6. Wang, M.; Yu, J. H.; Kaplan, D. L.; Rutledge, G. C. *Macromolecules* **2006**, *39*, 1102.
7. Reneker, D. H.; Yarin, A. L.; Fong, H.; Koombhongse, S. *J. Appl. Phys.* **2000**, *87*, 4531.
8. Yarin, A. L.; Koombhongse, S.; Reneker, D. H. *J. Appl. Phys.* **2001**, *89*, 3018.
9. Hohman, M. M.; Shin, M.; Rutledge, G.; Brenner, M. P. *Phys. Fluids*, **2001**, *13*, 2201.
10. Hohman, M. M.; Shin, M.; Rutledge, G.; Brenner, M. P. *Phys. Fluids* **2001**, *13*, 2221.
11. Thoppey, N. M.; Bochinski, J. R.; Clarke, L. I.; Gorga, R. E. *Polymer* **2010**, *51*, 4928.
12. Theron, S. A.; Zussman, E.; Yarin, A. L. *Polymer* **2004**, *45*, 2017.
13. Zhou, F.-L.; Gong, R.-H.; Porat, I. *J. Mater. Sci.* **2009**, *44*, 5501.
14. Srivastava, Y.; Loscertales, I.; Marquez, M.; Thorsen, T. *Microfluid. Nanofluid.* **2008**, *4*, 245.
15. Nayak, R.; Padhye, R.; Kyratzis, I. L.; Truong, Y. B.; Arnold, L. *Textile Res. J.* **2011**, *82*, 129.
16. Zheng, Y.; Liu, X.; Zeng, Y. *J. Appl. Polym. Sci.* **2013**, *130*, 3221.
17. Miao, J.; Miyauchi, M.; Simmons, T. J.; Dordick, J. S.; Linhardt, R. J. *J. Nanosci. Nanotechnol.* **2010**, *10*, 5507.
18. Khajavi, R.; Abbasipour, M. *ScientiaIranica* **2012**, *19*, 2029.
19. Kurban, Z.; Lovell, A.; Bennington, S. M.; Jenkins, D. W. K.; Ryan, K. R.; Jones, M. O.; Skipper, N. T.; David, W. I. F. *J. Phys. Chem. C*, **2010**, *114*, 21201.
20. Zhang, W. J. *J. Power Sources* **2011**, *196*, 13.
21. Chen, S.; Hou, H.; Hu, P.; Wendorff, J. H.; Greiner, A.; Agarwal, S. *Macromol. Mater. Eng.* **2009**, *294*, 265.
22. Han, X. J.; Huang, Z. M.; He, C. L.; Liu, L.; Wu, Q. S. *Polym. Compos.* **2006**, *27*, 381.
23. Haibao, Z.; Binrui, C.; Zipeng, Z.; Laxmi, A. A.; Dong, L.; Shaorong, L.; Chuanbin, M. *Biomaterials* **2011**, *32*, 4744.